Ibragimova, Rina; Puska, Martti J.; Komsa, Hannu Pekka

PH-Dependent Distribution of Functional Groups on Titanium-Based MXenes

Published in:
ACS Nano

DOI:
10.1021/acsnano.9b03511

Published: 01/01/2019

Document Version
Publisher's PDF, also known as Version of record

ACS NANO

Cite This: ACS Nano 2019, 13, 9171−9181

www.acsnano.org

ARTICLE

pH-Dependent Distribution of Functional Groups on Titanium-Based MXenes

Rina Ibragimova, Martti J. Puska, and Hannu-Pekka Komsa*

Department of Applied Physics, Aalto University, P.O. Box 11100, 00076 Aalto, Finland

Supporting Information

ABSTRACT: MXenes are a new rapidly developing class of two-dimensional materials with suitable properties for a broad range of applications. It has been shown that during synthesis of these materials the surfaces are usually functionalized by O, OH, and F and further suggested that controlling the surface allows controlling the material properties. However, a proper understanding of the surface structure is still missing, with a significant discrepancy between computational and experimental studies. Experiments consistently show formation of surfaces with mixed terminations, whereas computational studies point toward pure terminated surfaces. Here, we explain the formation of mixed functionalization on the surface of titanium-based two-dimensional carbides, Ti_2C and Ti_3C_2, using a multiscale modeling scheme. Our scheme is based on calculating Gibbs free energy of formation by a combination of electronic structure calculations with cluster expansion and Monte Carlo simulations. Our calculations show formation of mixtures of O, OH, and F on the surface with the composition depending on pH, temperature, and the work function. On the other hand, our results also suggest a limited stable range of compositions, which challenges the paradigm of a high tunability of MXene properties.

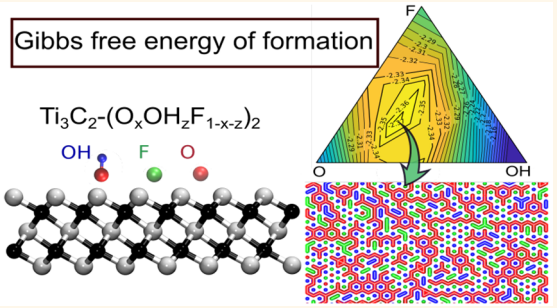

KEYWORDS: *2D materials, MXene, multiscale simulation, functional group, density functional theory*

Two-dimensional materials, such as graphene, molybdenum disulfide, and black phosphorus have been investigated intensely in recent years,[1,2] and related research efforts are moving to real applications. These materials are commonly prepared either by mechanical or chemical exfoliation or by deposition techniques.[3] A completely new class of 2D materials, called MXenes, consisting of early transition metals such as Ti, Sc, Zr, Hf, V, Nb, Ta, Cr, Mo (denoted as M), and carbon or nitrogen (denoted as X), has recently been drawing attention.[4] 2D MXenes provide suitable electronic, optical, and mechanical properties for a wide range of applications such as supercapacitors, battery electrodes, transparent conductive coatings, electromagnetic interference shielding, and optoelectronics.[5−8] MXenes are synthesized through etching of layered bulk phases, known as MAX phases, where transition metal carbide layers are connected by metal atoms, such as Al.[9] In the case of Ti_3C_2Al, selective etching with HF removes aluminum atoms by formation of AlF_3, and further sonication delaminates layers into $Ti_3C_2T_x$ flakes. During the synthesis, the surface adsorbs functional groups T = (OH, O, F), which play a crucial role on the overall MXene properties. Such tunability is a key difference between MXenes and the other 2D materials, especially as it opens a possibility to engineer the material properties *via* surface functionalization. Computationally, it has been shown that it should be possible to modify electrical and optical properties by a variation of surface termination, but this has been found to be challenging to achieve in experiments.

In the experimental reports, there are large variations in the obtained composition and distribution of functional groups even when the preparation is carried out under similar conditions.[10−16] This seems to stem from two factors: (i) the details of the functionalization mechanism and how it depends on the preparation conditions remain unclear, and (ii) it is difficult to obtain reliably quantitative information as the surface contains light elements, such as H and F, and is possibly in contact with a solution. Thus far, several experiments, such as the energy-loss microscopy,[17,18] thermogravimetric analysis,[12] neutron scattering,[19] and nuclear magnetic resonance spectroscopy (NMR),[20] have been conducted. NMR spectroscopy of Ti_3C_2 showed a mixing of O, F, and OH without any segregation in separate regions.[20] It has also been shown that the composition depends on concentration and type of etchants: O functionalization dominates when Ti_3C_2 is etched using a mixture of LiF and HCl,[20,21] and F functionalization dominates when using HF.[20]

First-principles calculations could provide the much-needed insight into the functionalization mechanism, but the results

Received: May 7, 2019
Accepted: August 8, 2019
Published: August 8, 2019

DOI: 10.1021/acsnano.9b03511
ACS Nano 2019, 13, 9171−9181

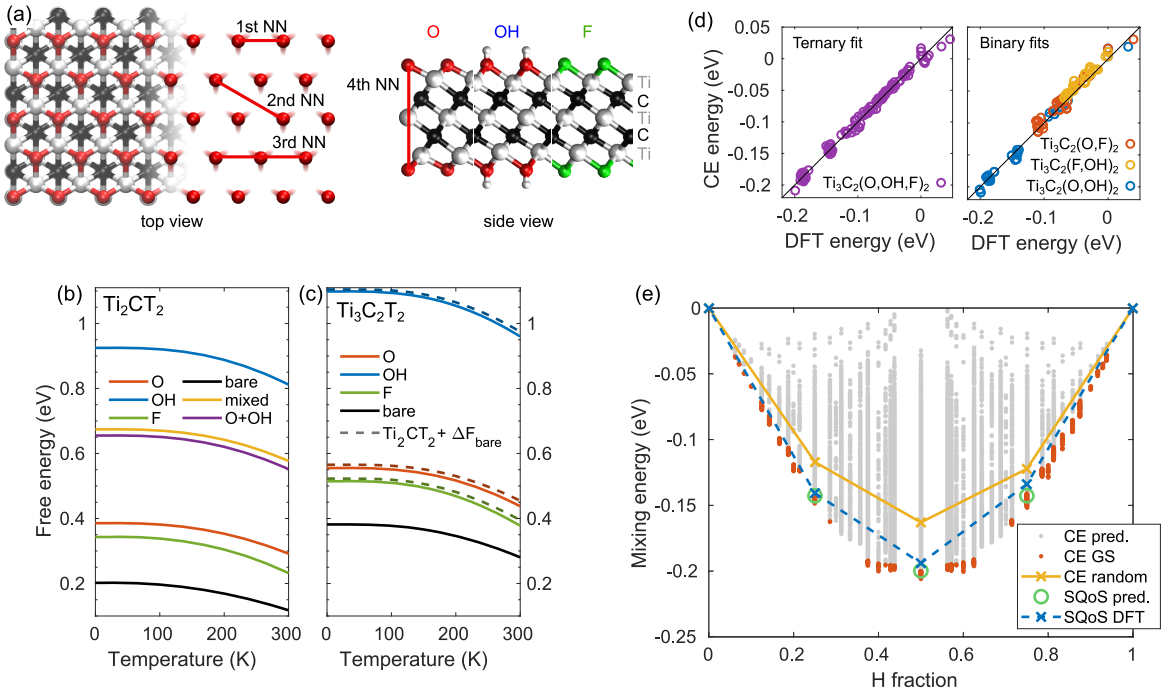

Figure 1. (a) **Atomic structure of $Ti_3C_2O_2$ in top view and of all pure terminations in side view. Clusters used in the expansion are denoted in the top view. (b,c) Phonon contributions to the free energy (per unit cell) for Ti_2C and Ti_3C_2 calculated in the cases of bare MXene and pure O-, OH-, and F-terminations. Moreover, in (b), the free energy from an explicit calculation for one of the mixed configurations and its approximation using the linear combination of the bare termination values are also shown. (d) Comparison of the DFT energy *vs* the predicted CE energy in the case of ternary and binary compounds. (e) Mixing energy for the $Ti_3C_2(O_xOH_{1-x})_2$ binary mixture. The gray points indicate predicted energies, and the red points highlight the ground states. The yellow crosses denote the CE energies for the purely random distributions; the green circles the CE energies for SQoS structures mimicking the distributions of functional groups obtained from the MC simulations at room temperature, and the blue crosses indicate the corresponding DFT energies.**

are still far from conclusive. This is a challenging problem as it requires an accurate description of the interactions between the MXene sheet, the functional groups, and the solution and a proper thermodynamic averaging in the case of mixtures. Almost all of the previous formation energy calculations have been carried out for pure terminations and yielded a strong preference for O-termination.[22−28] In order to model a mixture of terminations, MD simulations were carried out with an explicit solvent and found to yield predominantly F- and OH-terminations,[10] with the exact composition depending on the HF concentration. In addition, global structure optimization methods were employed to find the ground-state structure, in which case the comparison of formation energies showed predominantly O-terminations and no preference for mixing.[27] Only the studies focusing on hydrogenation[29,30] of O-terminated surfaces seem to suggest that the coverage can be tuned by pH or the electrode potential. Clearly, the surface structure inferred from the calculations is at odds with the experimental data showing a mixture of all three types of terminations. The origin of this discrepancy is still unclear but can arise from ignoring the role of the solvent,[31] an improper treatment of the chemical potential of elements,[32] and absence of thermodynamic sampling.[33] Thus, the important questions still remain: how functional groups are distributed and how the composition depends on the experimental conditions.

Here, we develop a computational scheme to find the composition and distribution of O, OH, and F functional groups on the Ti_2C and Ti_3C_2 monolayers at given experimental conditions. Our multiscale scheme is based on three steps. First, we adopt the cluster expansion (CE) method together with the density functional theory (DFT) to efficiently evaluate the energies of functional group configurations. Second, the CE model together with Monte Carlo simulations enables us to access the configurational free energies and to obtain distributions of the functional groups on the surface. Finally, we calculate the Gibbs free energy of formation in solution over the whole composition range, carefully accounting for the role of experimental factors, such as temperature, pH, and the work function. We also evaluate selected material properties and discuss the degree of tunability over the accessible range of compositions.

RESULTS

Benchmarking Computational Approach. Surface functionalization is a complex process involving different time scales and levels of physics. A proper consideration of surface interaction with adsorbants and solution is needed as the functionalization process happens in an etchant solution. On the other hand, a thermodynamically driven statistical averaging needs to be carried out in the case of mixed terminations. The need of a proper sampling of the configuration space leads us to combine electronic structure calculations and concepts of statistical mechanics and thermodynamics.

In order to compare the stabilities of MXene sheets with different surface terminations, we determine their Gibbs free energies of formation, which is obtained by finding the Gibbs free energies for all of the constituents. Here, we define it for the terminated MXT sheet with respect to the bare, unterminated MX sheet as

DOI: 10.1021/acsnano.9b03511
ACS Nano 2019, 13, 9171−9181

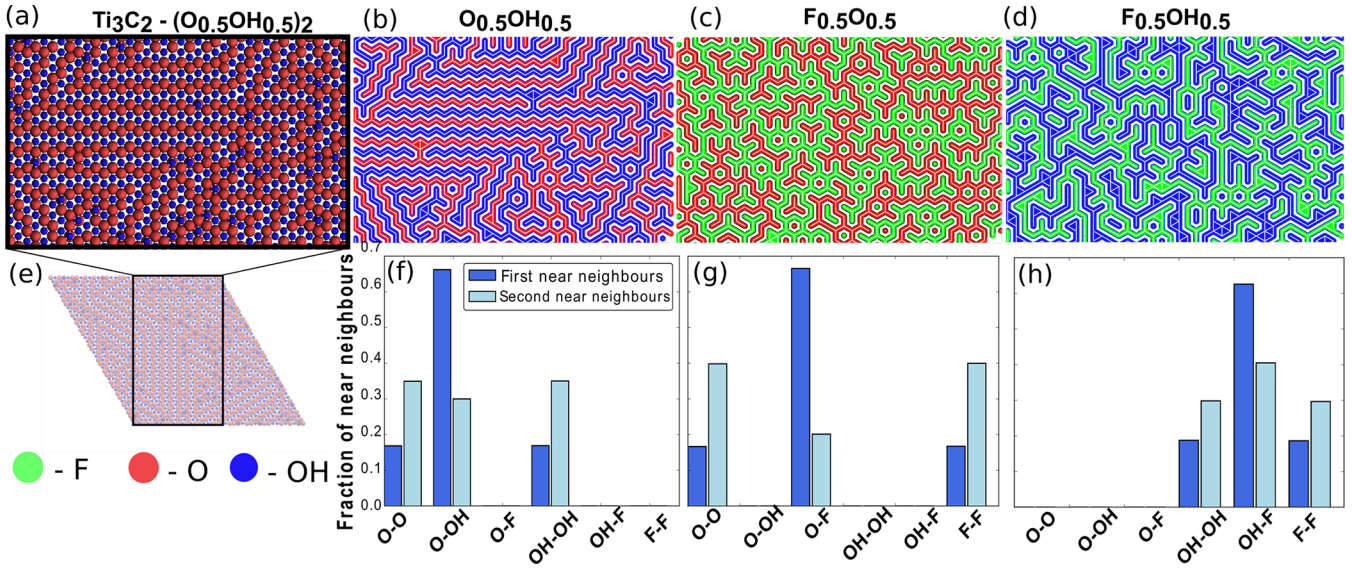

Figure 2. (b–d) Surface structures and (f–h) nearest neighbor fractions for (b,f) $Ti_3C_2(O_{0.5}OH_{0.5})_2$, (c,g) $Ti_3C_2(O_{0.5}F_{0.5})_2$, and (d,h) $Ti_3C_2(OH_{0.5}F_{0.5})_2$. In (b–d), the nearest neighbor atoms of the same type are connected by bonds to highlight the ordering. (a,e) Shows the structure in panel (b) without the connections and also illustrates how the rectangular region is cut from the larger Monte Carlo simulation cell.

$$\Delta_f G^\circ(\mathrm{MXT}) = G^\circ(\mathrm{MXT}) - G^\circ(\mathrm{MX}) - \sum_i n_i \tilde{\mu}_i \quad (1)$$

where n_i is the number of termination atoms of type i and $\tilde{\mu}_i$ is their chemical potentials.[34] G is the "total" Gibbs free energy of the system including configurational and vibrational contributions and the interaction with the solvent. All three contributions are important. They are evaluated here separately and added to the total energies calculated with DFT. The "°" refers to the standard conditions: room temperature and in solution with pressure p = 1 atm. The chemical potentials for adsorbed species at these conditions are determined by combining DFT total energies and experimentally determined changes in enthalpy and entropy, as described in detail in Methods.

In order to access the configurational free energies of MXenes with mixed terminations, we construct a lattice-gas Hamiltonian, which is then used in Monte Carlo simulations. For the lattice-gas Hamiltonian, we use the CE defined by a series of interactions between atoms at different lattice sites and multiplied by constant expansion coefficients (effective cluster interactions, ECI). The ECIs in the cluster expansion are usually obtained *via* fitting the CE energies to those calculated by DFT for a set of configurations. Here, we generate CE for the three-component (O, OH, F) mixture by fitting to a set of 71 and 106 DFT energies for Ti_2C and Ti_3C_2, respectively. After evaluating different expansions, we choose for Ti_3C_2 a CE including pair clusters up to the fourth nearest neighbors and triplet clusters up to the first nearest neighbors, which corresponds to a total of 13 pair clusters and 4 triplet clusters after accounting for the symmetry of the lattice and the dimension of the configuration space in a three-component alloy. The pair clusters up to fourth nearest neighbor were sufficient in the case of Ti_2C. These choices yielded small cross-validation scores of 0.008 and 0.005 eV/atom for Ti_3C_2 and Ti_2C, respectively. Used clusters are illustrated in Figure 1a. The quality of the cluster expansion is demonstrated in Figure 1d, where we compare the DFT energy to the energy predicted using the CE. The ternary compound panel essentially includes all of the structures that were used in the fitting process. In addition, we carried out a separate set of DFT calculations for binary compounds, where each type of compound included a large number of configurations that were not present when training the expansion. The ability for the CE to predict the energies of these previously unencountered configurations illustrates the good transferability of the expansion. Using the obtained CE, we can quickly evaluate the total energies for a large number of configurations or for larger supercells. Figure 1e shows the energies evaluated for a large set of configurations in the O–OH binary system (gray dots). Also shown are the energies expected for the purely random mixtures (yellow crosses) and the average energies (green circles) for the system at room temperature, as obtained from Monte Carlo simulations.

Finally, we highlight the importance of the vibrational free energy contributions in Figure 1b,c. It shows a significant contribution of nearly 1 eV, which obviously cannot be neglected in the calculation of the Gibbs free energy of formation. It mostly arises from the zero-point energy, whereas the change upon approaching room temperature is only about 0.1 eV in all cases. The large difference between OH- *versus* O- and F-terminations arises from the very high frequency of O–H vibrations. Comparison of the Ti_2CT_2 and $Ti_3C_2T_2$ results reveals that each termination yields very similar free energy contribution; that is, the differences between the three curves are the same. This suggests that each terminating atom/group has a fixed contribution to the free energy, and thus for a mixed surface, we could use the free energies from the pure terminations weighted according to the composition. This is demonstrated in Figure 1b, which shows the results for the mixed $Ti_2C(O_{0.5}OH_{0.5})_2$ configuration. Taking the weighted average of pure terminations yields a free energy contribution differing from the explicit calculation by only about 20 meV.

Simulated Surface Distribution of Functional Groups. Surface distributions of functional groups for Ti_2C and Ti_3C_2 are obtained using Monte Carlo and the CE constructed earlier. We use the canonical ensemble, where the concen-

DOI: 10.1021/acsnano.9b03511
ACS Nano 2019, 13, 9171–9181

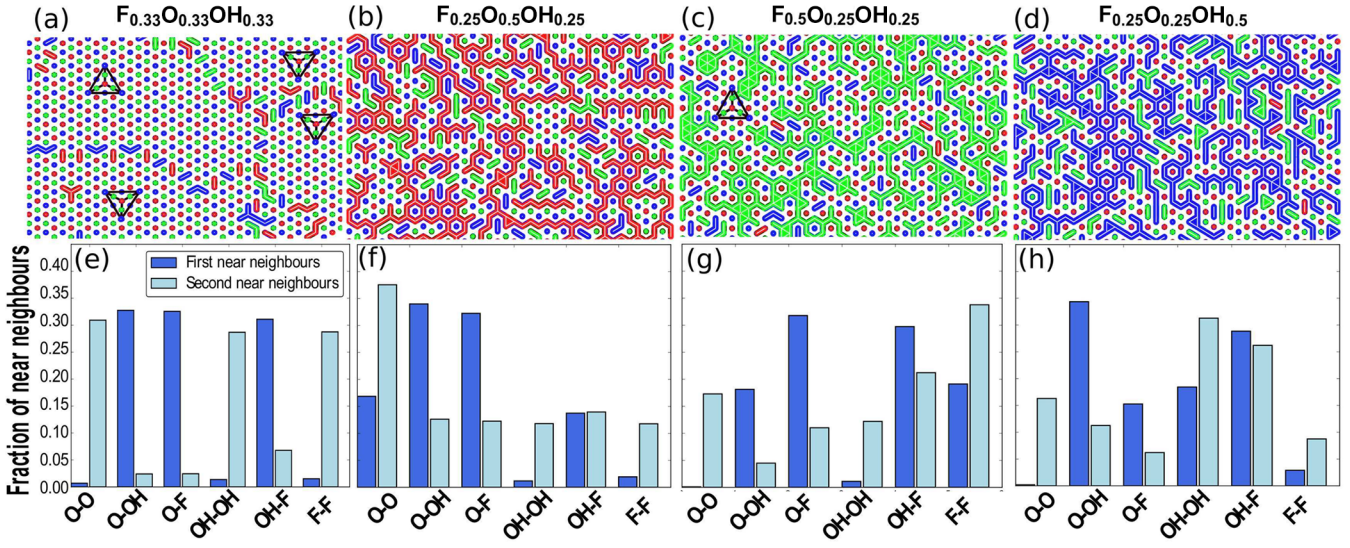

Figure 3. (a–d) Surface structures and (e–h) nearest neighbor fractions for (a,e) $Ti_3C_2(O_{0.33}OH_{0.33}F_{0.33})_2$, (b,f) $Ti_3C_2(O_{0.5}OH_{0.25}F_{0.25})_2$, (c,g) $Ti_3C_2(O_{0.25}OH_{0.25}F_{0.5})_2$, and (d,h) $Ti_3C_2(O_{25}OH_{0.5}F_{0.25})_2$. In (a,c), the triangles illustrate the orientation of the ordered phases.

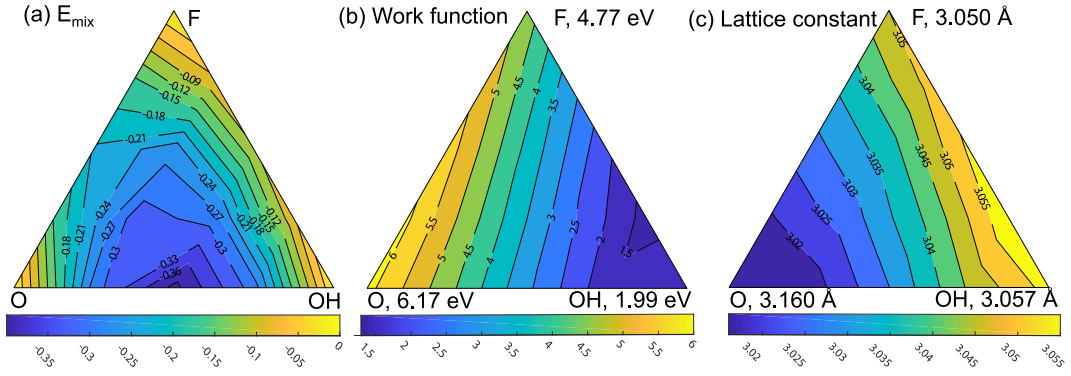

Figure 4. (a) Mixing energy (in eV and per MXene unit cell containing two surface sites), (b) work function (in eV), and (c) lattice constant of Ti_3C_2 (in Å) as a function of the alloy composition. In (b,c), the numerical values for the end points are listed.

tration of surface adsorbants is fixed. MC simulations are conducted for 12 structures with different compositions: Ti_3C_2-$(O_xOH_zF_{1-x-z})_2$, where x and z vary from 0 to 1 with a step of 0.25. We first show in Figure 2b–e the surface structures for equal concentrations of two functional groups (*i.e.*, a binary mixture) on Ti_3C_2. We have postprocessed the obtained structures by continuously coloring the first nearest neighbors of the same type (Figure 2b–d). Fairly similar striped patterns are observed in all cases typical for strongly mixing species in a triangular lattice, which is a frustrated system. Figure 2f–h shows the corresponding fractions of the first and second nearest neighbors averaged over the simulation cell. Independent of the constituents, the first nearest neighbor distributions show very similar fractions of about 0.18 between the "like"-terminations and about 0.65 between the "unlike"-terminations. In a random alloy, the values would be 0.25 and 0.5, respectively, meaning that unlike neighbors are overall favored. This, together with the comparison of the energies for the random and MC (SQoS) results in Figure 1e, clearly shows that the surface terminations are not expected to be randomly distributed. The second nearest neighbor fractions show the opposite trend, wherein similar terminations are more likely than in random alloys. This effect is particularly pronounced in the case of $O_{0.5}F_{0.5}$, which may explain the slightly different visual appearance.

Figure 3 shows the MC-simulated distribution of functional groups and the nearest neighbor fractions for selected ternary structures. We start off with an equal concentration for each of the three groups, as shown in Figure 3a. Although a binary system in a triangular lattice is frustrated, a ternary (three-state) system is not. As seen in Figure 3a, large areas of the ordered phase, where each O is surrounded by 3 F and 3 OH, *etc.*, arise. This is also reflected in the fractions showing almost completely unlike-terminations in the nearest neighbor sites in Figure 3e. It is interesting to note also the phase boundary structure, as highlighted by the triangles in Figure 3a, where we can identify two types of boundaries: those where the ordering of the terminations is inverted and those where the ordering is the same, but the pattern is shifted between the two grains.

Surface distribution for a mixture with excess O $[Ti_3C_2(O_{0.5}OH_{0.25}F_{0.25})_2$ in Figure 3b] shows a formation of oxygen containing zigzag stripes, whereas OH and F mostly form triangular structures, where a central atom is surrounded by three atoms of another type. The same kind of arrangement of functional groups can be seen on the surface with excess OH $[Ti_3C_2(O_{25}OH_{0.5}F_{0.25})_2$ in Figure 3d]. The first and second nearest neighbor fractions show the same tendency for excess O and excess OH (Figure 3f,h), where the first nearest neighbors appear to be unlike-terminated, and the second nearest neighbors are like-terminated. This is fully consistent

DOI: 10.1021/acsnano.9b03511
ACS Nano 2019, 13, 9171–9181

with the results from the binary compounds in Figure 2. The surface with excess F [$Ti_3C_2(O_{0.25}OH_{0.25}F_{0.5})_2$ in Figure 3c] shows a larger number of fluorine atoms that have agglomerated to small clusters, whereas the remaining surface still shows the ordered distribution. Thus, in all of the cases examined here, the surface terminations strongly favor mixing and do not segregate.

For Ti_2C, the results are shown in the Supporting Information and exhibit overall very similar trends.

Properties of Mixed Terminations. Next, we study the properties of these mixtures by carrying out DFT calculations for the best representative structures in smaller supercells created using the special quasi-ordered structures (SQoS) scheme, which is based on mimicking cluster correlations in MC simulations. The mixing energies, lattice constants, and work functions as a function of the composition are shown in Figure 4. We find large mixing energies in accordance with the mixed distributions in Figures 2, 3, and 1e. The largest energy gain is found with O- and OH-terminations without any F and reaching almost −0.4 eV per unit cell. This is a very large energy gain and clearly much more than k_BT for temperatures used during etching and delamination. In the case of O/F and F/OH mixings, the maximum energy gains are −0.21 and −0.09 eV, respectively. According to Hu *et al.*, the O- and OH/F-terminations lead to oppositely charged Ti-(O/C/F) octahedra within the MXene sheet,[35] thereby favoring alternating terminations. We propose that there is an additional contribution arising from the fact that in the case of OH the outermost H atom is positively charged, whereas in the case of O and F, the outermost atoms are negatively charged, which leads to attractive electrostatic interaction. Adding the solvation energy to the mixing energy only makes the mixing more favored, as shown in the Supporting Information. In the case of Ti_2C, the energy surface is overall very similar, but the mixing energies are somewhat smaller, reaching up to −0.3 eV per unit cell.

The work functions are shown in Figure 4b. The OH functionalization leads to a very low work function, whereas the work function is high for the O-terminated surface. The Ti_2C results are very similar to those for Ti_3C_2, thereby suggesting that the work function is termination-specific and not material- or composition-specific. The calculated work functions of terminated Ti_2C and Ti_3C_2 coincide with earlier calculated work function values reported in ref 36, where it was also found that the work function has a very weak dependence on the layer thickness; that is, it originates largely from the surface dipole formation due to terminating groups and not from changes in the Fermi level. The high work functions of the O- and F-terminated surfaces are due to charge transfer to these sites, whereas the low work function of OH-terminated surface is due to the intrinsic dipole moment (and possibly due to relaxation effect).[36] There is no obvious correlation between the mixing enthalpy and the work function, which indicates that mixing is not governed by the work function, but it is likely related to the electrostatics between the terminations, as discussed above.

Measuring of work function is generally challenging, and it is particularly difficult to simultaneously determine the surface termination composition. For Ti_2C, very few experiments are available due its instability: for $Ti_2COH_xF_y$, a work function of 4.98 eV is reported.[37] Experimental work functions for Ti_3C_2 vary from 3.4 up to 5.28 eV. A work function of 3.4 eV is reported for predominantly OH-terminated sheets.[38] Work functions of 4.37 and 4.6 eV are reported in refs 39 and 40. The highest work function has been reported in ref 16, and although the exact termination is unknown, it was proposed to arise from protonization of OH with the presence of water, resulting in formation of O. Nevertheless, none of these values are close to the calculated limits of 2.0 eV for pure OH-terminated Ti_3C_2 or 6.2 eV for pure O-terminated Ti_3C_2, which suggests that the measured samples feature mixing. We note that when the experimental work function is known, one can extract from Figure 4b a fairly good estimate for the amount of OH, although the O/F balance still remains unknown.

Finally, the lattice constants in Figure 4c appear to closely follow Vegard's law. Whereas experimentally determined in-plane lattice constant values have been reported in a few papers, comparison is difficult because (i) in calculations, the accuracy of the lattice constants is unknown even though the composition is known exactly, and (ii) in experiments, the composition is often unknown even though the lattice constant might be known fairly accurately.

Gibbs Free Energy of Formation. In the previous section, we obtained large negative mixing energies which strongly pointed toward mixing. However, the mixing energies are not enough to predict the composition under thermodynamic equilibrium. For that, we evaluate the Gibbs free energy of formation with carefully chosen chemical potentials.

While during the functionalization the H atom can be adsorbed from H^+ or H_2 or H_2O, under equilibrium conditions, the chemical potential for H in all of these different species is the same. The value for the chemical potential will be determined by the amount of dissolved HF (*i.e.*, pH), temperature, the equilibrium with water [$\mu(H_2O) = \mu(O) + 2\mu(H)$], and the electron chemical potential in the case of ionic species. Chemical potentials as a function of electron chemical potential (work function Φ) for two values of pH under ambient conditions are shown in Figure 5, where

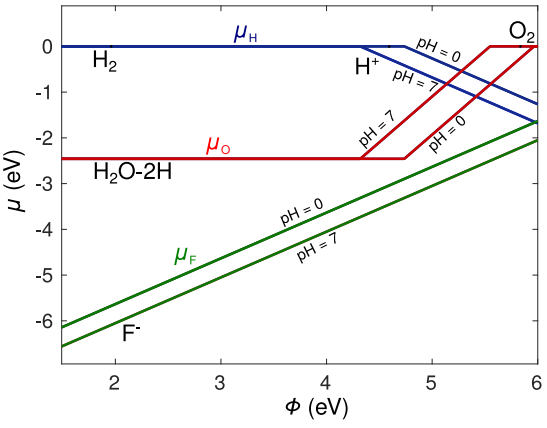

Figure 5. Chemical potential of O, F, and H depending on work function.

we only show the lowest energy species at given conditions. Under the conditions present during the MXene synthesis, these correspond to H coming from H_2 or H^+ depending on conditions, F from F^-, and O from H_2O. From the crossing point of $\mu(H)$ lines corresponding to H_2 and H^+ (pH = 0), we obtain a calculated value for the standard hydrogen electrode (SHE) of −4.7 eV, which is in good agreement with other

DOI: 10.1021/acsnano.9b03511
ACS Nano 2019, 13, 9171−9181

computational works[34,41] and in fair agreement with the experimental value of −4.44 V.[42]

Using the calculated chemical potentials of O, OH, and F, we can construct the formation Gibbs free energies of pure terminations as a function of the electron chemical potential and pH. These are shown in Figure 6, where the calculated work functions are also indicated. Simply finding the lowest energy phase at the respective value of Φ would seem to indicate the formation of a fully O-terminated surface. This, however, leads to few problems. A work function of 6.1 eV (or +1.4 V *vs* SHE) is extremely high, even outside the stability range of water and thus breaking water to O_2. Dissolved O_2 molecules are known to lead to oxidation of MXenes to TiO_2.[43,44] Moreover, it is simply at odds with the experimental reality that always shows a mixture of terminations.

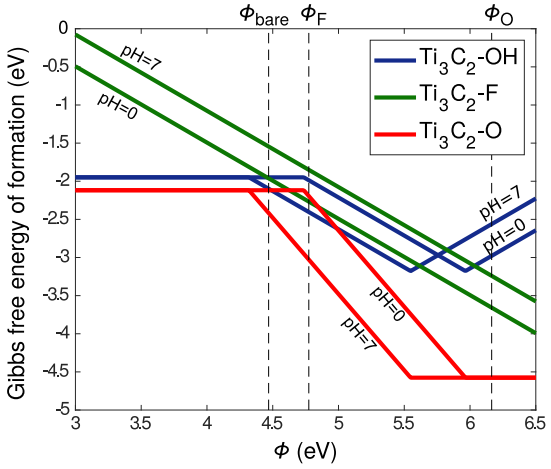

Figure 6. Gibbs free formation energy of pure OH-, F-, and O-terminated Ti_3C_2 depending on work function and pH of the solution.

However, that is not the only choice for the work function. First of all, it is important to make a difference between the work function of the final fully terminated surface and the work function during etching. One could argue that because the terminating group is adsorbed on a bare surface, the work function of a bare surface would be the most realistic choice. In addition, it is quite likely that the system is not under charge equilibrium. Extra electrons can arise from F^-, either upon adsorption or upon AlF_3 formation, and from breaking of H_2 to $2H^+$, which are then accumulated to the MXene sheet, thereby lowering the work function. F^- adsorption should occur frequently during the etching, as evidenced by the sizable concentration of F-terminations. The rate of H_2 to $2H^+$ events is not known, but it should only be relevant at a work function higher than SHE. On the other hand, electrons can be depleted by adsorbing H^+, either changing the O-termination to the OH one or forming H_2, which thereby increases the work function until it reaches SHE. Indeed, etching of MXenes is known to lead to H_2 gas formation.[11,45] Putting both of these aspects together, we suggest that most of the functionalization happens near the SHE conditions. In the end, using our selected etching work function, we obtain the composition and the corresponding work function for the terminated surface, which can be

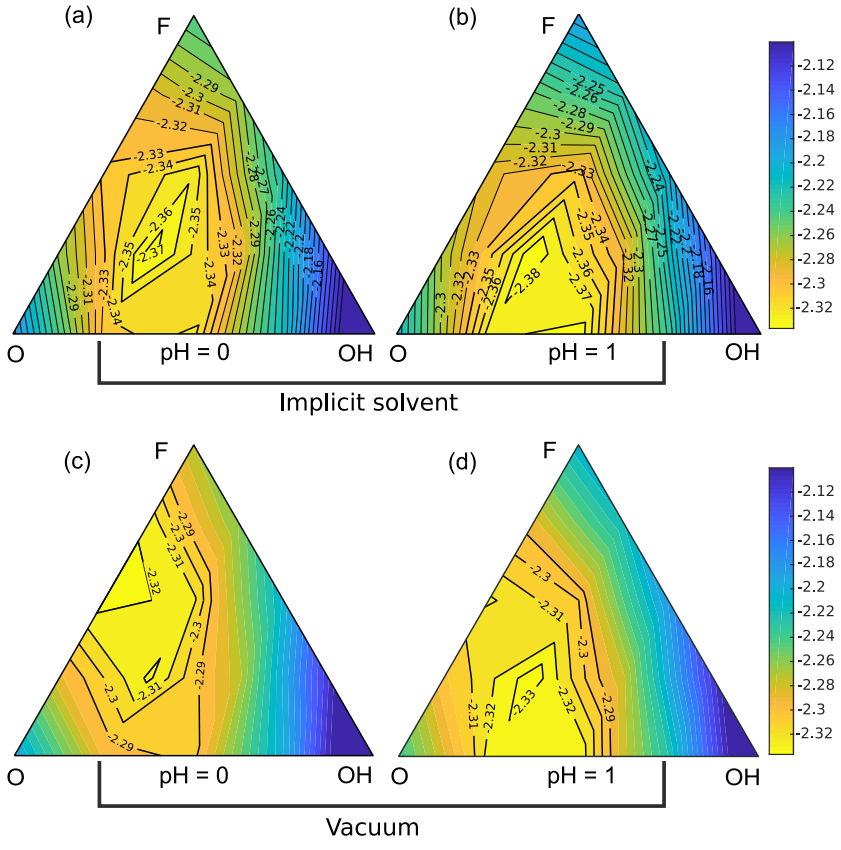

Figure 7. Gibbs free energies of formation for mixed terminations at the work function Φ = 4.7 eV including implicit solvents with (a) pH = 0 and (b) pH = 1, as well as the vacuum cases for (c) pH = 0 and (d) pH = 1.

DOI: 10.1021/acsnano.9b03511
ACS Nano 2019, 13, 9171−9181

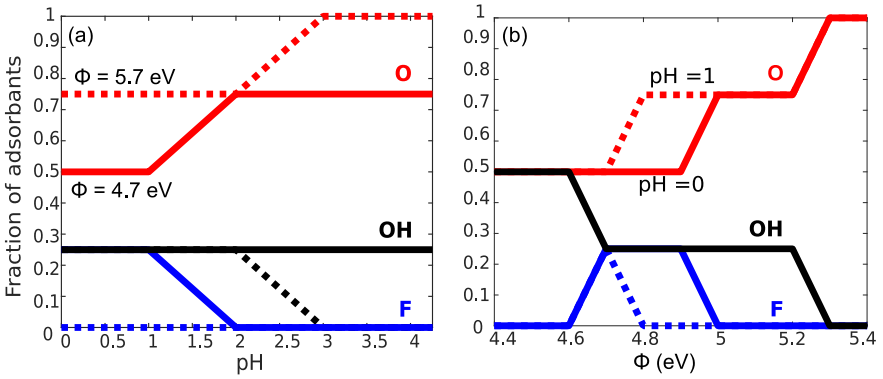

Figure 8. Lowest energy surface adsorbant concentrations depending on pH (a) and lowest energy surface adsorbant concentrations depending on the work function (b).

compared to the experimentally measured ones to check for consistency.

We calculated the Gibbs free energies of formation for the SQoS structures obtained earlier at a fixed work function and pH. Figure 7a,b shows the ternary diagrams of Gibbs free energy of formation for mixed surface terminations at a fixed work function equal to 4.7 eV and (a) pH = 0 or (b) pH = 1, which are typical values during the MXene synthesis. For comparison, we also show in Figure 7c,d the same cases, but in vacuum, that is, excluding the solvation energy contribution. Inspecting the numbers around the energy minimum reveals that the solvation energy contribution is relatively minor, some tens of millielectronvolts, but it tends to lower the energy of mixed configurations relative to the pure constituents. Generally, in all cases, the energy minima are found inside the triangles and are quite significantly lower in energy than those for the pure terminations. In vacuum, the $O_{0.5}F_{0.5}$ structure has the lowest Gibbs free energy at pH = 0, but the energy surface is very flat between this point and $O_{0.5}OH_{0.5}$. The change of pH to 1 shifts the minimum energy to the $O_{0.5}F_{0.25}OH_{0.25}$ mixture. When solvation is included, the energy minimum lies in both cases close to $O_{0.5}F_{0.25}OH_{0.25}$. Due to the flatness of the energy surface between $O_{0.5}F_{0.5}$ and $O_{0.5}OH_{0.5}$, even a small solvation energy contribution is sufficient to shift the location of the energy minimum. Such sensitivity means that our calculations may not be able to predict the exact composition but only the dominant stability region.

In Figure 8a, we show how the composition at a fixed Φ changes as pH is varied. The OH concentration remains near 0.25, but for pH >1, the concentration of O increases and that of F decreases; that is, the minimum of Gibbs free energy shifts to the composition $O_{0.75}OH_{0.25}$. This is consistent with the hydrogenation study by Zhan *et al.*, showing H coverage of about 0.3 when the point of zero charge is close to SHE.[29] Finally, we have also varied the work function Φ from 4.4 to 5.4 eV and plotted the composition in Figure 8b. At low work function values, we obtain $O_{0.5}OH_{0.5}$, largely independent of pH (also see Figure 6). At very large work function values, the pure O-terminated surface is obtained. Only at intermediate values is it possible to obtain mixtures with marked F concentrations.

DISCUSSION

In this study, we have combined multiple theoretical approaches to simulate functionalization of the Ti_3C_2 and Ti_2C surfaces. Surface distributions of functional groups over distinct concentrations have been obtained. We have shown that functional groups are equally distributed without any segregation regardless of the concentration or the type of the adsorbant. Our simulation results align with recent experimentally measured data,[17,20] where random distributions of terminations were reported. The preference toward mixing arises from the significant energy gain by mixing and has been obtained by accounting only structural factors (Figure 4a). On the other hand, the lowest energy composition of the functional groups on the surface varies with the electrochemical factors such as the electron chemical potential Φ, pH, and temperature. We showed that the lowest energy composition is sensitive to these parameters, but when choosing values similar to those in experiments, we obtained similar mixtures of all three components as reported in experiments. Now, taking the obtained compositions and referring to Figure 4b, the low Φ composition, $O_{0.5}OH_{0.5}$, corresponds to a work function of about 3.5 eV, which is close to the lower limit obtained in experiments.[38] The composition $O_{0.5}F_{0.25}OH_{0.25}$ would result in a work function of about 4.5 eV, which is consistent with those reported in refs 39 and 40, whereas the high Φ or high pH composition $O_{0.75}OH_{0.25}$ leads to a work function closer to 5 eV, similar to that reported in ref 16.

When comparing our calculated composition to experimental ones, the problem is that one can find experimental report to support any computational finding: similar concentration of all three terminations in ref 46, O dominance in ref 18, F dominance in refs12 and 15, equal O and F *versus* small OH concentration in ref 20, equal F and OH *versus* small O concentration in ref 19. Perhaps the most useful reports are those which report composition changes upon changing synthesis conditions. For instance, according to Wang *et al.*, going from a 10% HF concentration to 48%, the O/F ratio decreases from 1.4 to 0.8,[19] which qualitatively agrees with our result that lower pH increases the F concentration. Although the high sensitivity of the functional group composition to the experimental conditions may explain part of the results, there are some discrepancies. Our calculations always resulted in an O concentration of 50% or more and a relatively small F concentration of 25% or less. The possible reasons could include local variations in the solution (content of F^- ions, trapped H_2, *etc.*), kinetic factors related to etching, and inaccuracies in our computational approach.

DOI: 10.1021/acsnano.9b03511
ACS Nano 2019, 13, 9171−9181

Although it seems that the surface composition can be tuned, even if only within a limited range, how would that affect the material properties, such as the electrical conductivity? We show the total and atom-projected densities of states in Figure 9, where we have also indicated the atomic

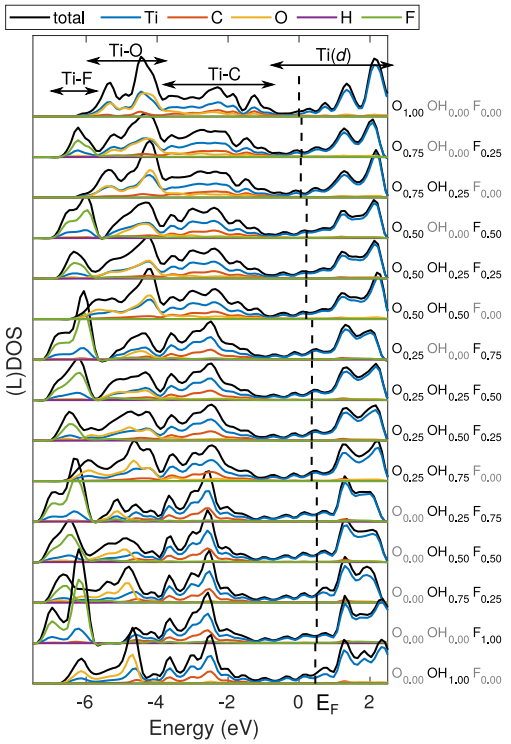

Figure 9. Atom-projected density of states from all Ti_3C_2 SQoS. The vertical dashed line indicates the Fermi level position.

origins of all the main features. The Fermi level moves down as the concentration of O increases, as expected due to its large electronegativity and oxidation state. Nevertheless, the Fermi level is always confined inside the Ti-d band, and moreover, this band is largely unaffected by the surface terminations and appears fairly similar in all cases. Thus, there is likely no dramatic changes in the density of states at the Fermi level or consequently in the electrical conductivity (assuming it is governed by the former), especially if considering only the limited range of compositions. The situation is again very similar in the case of Ti_2C (Figure S7). Whereas pure O-terminated Ti_2CO_2 should open a band gap at the Fermi level, so far, there are no experimental reports on the synthesis of pure Ti_2CO_2, and our calculations show that mixing is again strongly favored (Figure S5), thereby suggesting that synthesis of Ti_2C with pure O-terminations is difficult. As a result, our findings cast doubt on the proposed wide tunability of the surface composition and electronic properties of Ti-based MXenes and also suggest that calculations based on surfaces with pure terminations may not provide reliable predictions of MXene properties.

CONCLUSIONS

In this study, we have shown that functional groups form mixed compositions at Ti_2C and Ti_3C_2 surfaces. Our large-scale simulations show that mixed functional groups are equally distributed at the surfaces and form ordered arrangements for certain concentrations. Furthermore, we have constructed Gibbs free energy diagrams for different concentrations of functional groups depending on pH and the work function. The analysis shows that formation of mixed terminations is favorable. Our results show that the tunability of the surface composition by pH and temperature is limited, and it does not lead to dramatic changes in electronic properties. Our multiscale modeling approach for determining the distribution and composition of functional groups on a surface should be straightforward to apply to other MXene systems in order to more accurately predict their structures and properties. Moreover, many other systems, other than MXenes, can be considered, especially those of solvated nanoparticles.

METHODS

Free Energy Calculations. The Gibbs free energy of formation is given in eq 1. The free energy of the sheet should include the vibrational contributions as well as the interaction with the solution. We assume that the two contributions do not depend on each other and thus

$$G^\circ(\mathrm{MXT}) = E(\mathrm{MXT}) + \Delta_{\mathrm{vib}}F(\mathrm{MXT}) + \Delta_{\mathrm{sol}}E(\mathrm{MXT}) \quad (2)$$

where $E(\mathrm{MXT})$ is the DFT total energy, $\Delta_{\mathrm{vib}}F$ is the phonon contribution to the free energy at room temperature evaluated in vacuum, and $\Delta_{\mathrm{sol}}E$ is the solvation energy evaluated at $T = 0$ using implicit solvation models. (The pV term can be ignored at $p = 1$ atm.)

The choice of chemical potentials μ_i depends on the conditions around the MXene sheet and the reactions on the surface. Taking as an example one of the most studied MAX phases, Ti_3AlC_2, when the etching is done in water solutions of HF, the following three simplified reactions have been proposed to take place:[11]

$$Ti_3AlC_2 + 3HF = AlF_3 + \frac{3}{2}H_2 + Ti_3C_2 \quad (3)$$

$$Ti_3C_2 + 2H_2O = Ti_3C_2(OH)_2 + H_2 \quad (4)$$

$$Ti_3C_2 + 2H_2O = Ti_3C_2(O)_2 + 2H_2 \quad (5)$$

$$Ti_3C_2 + 2HF = Ti_3C_2F_2 + H_2 \quad (6)$$

In these reactions, hydrogen is always assumed to be in the form of H_2. However, considering that HF dissociates in water to H^+ (or H_3O^+) and F^- ions, it seems plausible that the reactions could involve just the ions, an aspect that has not been accounted for in the previous studies on MXenes. In this work, we will consider both scenarios, which, thanks to the adopted method, is only reflected in the choice of the chemical potentials.

The chemical potentials are obtained by first evaluating the Gibbs free energies of the elemental phases using DFT and then using experimentally determined thermochemical quantities to evaluate Gibbs free energy of the solutes and the solution. Taking O_2 as an example, the DFT energy $E^{\mathrm{DFT}}(O_2)$ sets the (absolute) energy scale, which allows us to write the (absolute) enthalpy and Gibbs free energy of the molecule as

$$H^\circ(O_2) = E_{\mathrm{DFT}}(O_2) + E_{zp}(O_2) + \Delta H^\circ(O_2) \quad (7)$$

$$G^\circ(O_2) = H(O_2) - TS^\circ(O_2) \quad (8)$$

where E_{zp} and ΔH° are the zero-point vibrational energy and the enthalpy of formation for the molecule (similarly for H_2 and F_2), respectively. Then, the Gibbs free energy, or the chemical potential, of water is obtained as $\mu(H_2O) = \mu(O) + 2\mu(H) + \Delta_f G(H_2O)$, where the formation energy is obtained from the NIST-JANAF tables. On the other hand, if H is in the form of H^+ ions, we also need to consider the electron chemical potential. The formation energy of H^+ ion is written as

$$\Delta_f G(H^+) = \Delta_f G^\circ(H^+) - \mu(H) + \mu_e \quad (9)$$

DOI: 10.1021/acsnano.9b03511
ACS Nano 2019, 13, 9171−9181

where μ_e is given with respect to vacuum, that is, $\mu_e = \tilde{\mu}_e - \tilde{\mu}_e^{vac}$. The energy of solvated ions is obtained from the ion heat of formation in the gas phase plus the hydration energy. The ion heats of formation are taken from the NIST-JANAF thermochemical tables and the hydration energies from refs 47 and 48. We may also connect this to pH, which is directly related to the H^+ concentration in the solution:

$$c_{H+} = c_0 \cdot \exp(-\Delta_f G(H^+)/k_B T) = 10^{-pH} \quad (10)$$

where $c_0 = 55.55$ mol/L is the concentration of the H_2O molecules in water. Equations for F^- are similar. A full account of the chemical potential calculations and a list of all the thermochemical quantities are given in Supporting Information.

Computational Details. Our density functional theory calculations were carried out in the framework of projector-augmented waves as implemented in the VASP software package.[49] For the exchange-correlation functional, we wanted to choose one that properly reproduces the formation energies of MXenes. However, because experimental values are not available, we used TiO_2 and water for benchmarking. A full comparison of the heats of formation calculated using the computational scheme described above and the respective experimental values are given in Supporting Information. Among the considered functionals (PBE,[50] PBE-D3(BJ),[51] PBEsol,[52] PBEsol-D3(BJ), HSE06,[53] SCAN,[54] and SCAN+rVV10[55]), PBEsol seemed to give the best overall agreement with the experimental enthalpy of formation. Therefore, the MXene sheets were then calculated using the PBEsol functional.[52] The optimal plane-wave cutoff energy was chosen as 550 eV according to a convergence test. The set of 15 × 15 × 1 *k*-points was found to be sufficient for the unit cells of Ti_2C and Ti_3C_2.

Our calculated lattice constants and work functions are in good agreement with previous calculations for the fully terminated Ti-based MXenes.[24,56−58] The calculated lattice parameters and work functions are listed in Table 1. The lattice constant has been measured for Ti_3C_2 and is equal to 3.050 Å.[13]

Table 1. Calculated Lattice Parameters for Terminated Ti_2C and Ti_3C_2 Sheets

	Ti_2C	Ti_2CO_2	Ti_2COH_2	Ti_2CF_2
a, Å	3.040	3.006	3.040	3.026
Φ, eV	4.59	5.84	1.96	4.88
	Ti_3C_2	$Ti_3C_2O_2$	$Ti_3C_2OH_2$	$Ti_3C_2F_2$
a, Å	3.081	3.016	3.057	3.050
Φ, eV	4.47	6.16	1.99	4.77

Phonons and thermal properties were calculated using Phonopy.[59] The force constants were evaluated using a 5 × 5 supercell and the thermal properties integrated in 1000 × 1000 *k*-point mesh.

Solvation energies were calculated using VASPsol.[60,61] A high cutoff energy is required to properly describe the interfacial region between the implicit solution and the surface, in particular, to construct an appropriate grid for the cavity surface, and therefore, these calculations are carried out using a cutoff energy of 1000 eV. We keep the atomic positions fixed to those obtained from vacuum calculations. For the pure terminations, the solvation energies are very small: −50, −8, −40, and −9 meV for Ti_2C, Ti_2CO_2, Ti_2COH_2, and Ti_2CF_2, respectively. For the mixed configurations, we did not assume that the solvation energy contributions could be obtained using the pure terminations and averaging them according to the composition. Instead, we carried out explicit calculations for the solvation energies of the SQoS structures with the atomic structure fixed to that in vacuum.

The electron chemical potential μ_e is evaluated from the work function of the unsolvated sheets (in vacuum) for each of the three surface terminations.

Cluster Expansion of Alloy Energies, Monte Carlo Simulations, and Special Quasi-ordered Structures. Cluster expansion study for the mixture of surface terminations was carried out using ATAT.[62,63] In order to sample the configuration space, we generate CE for the three-component (O, OH, F) mixture by fitting to a set of 71 and 106 DFT energies for Ti_2C and Ti_3C_2, respectively. In addition to atomic positions, we also optimized the lattice constants. However, accurate effective cluster interactions require high-quality DFT data as well as the right selection of the number and type of clusters. For Ti_3C_2, we have considered clusters with 3, 6, 10, and 13 pairs and 4 triplets, as well. The set of 3 pair clusters includes only the first near neighbor interactions and basically resembles the Ising model. The sets of 6 and 10 clusters include interactions of the lateral first nearest neighbors as well as interactions between nearest neighbors on the opposite sides of the slab. The set of 13 pairs and 4 triplets includes lateral pair interactions up to the second nearest neighbor and the first nearest neighbor on the opposite sides of the slab. CE predicted energies are fitted using the least-squares method to the calculated DFT energies. The fitting quality was evaluated by the cross-validation (CV) score and by the residual distribution. Residuals were normally distributed in all cases. A small CV was obtained when including a set of 13 pair and 4 triplet clusters, that is, 0.008 eV/atom for Ti_3C_2 and 0.005 eV/atom for Ti_2C when including a set of 13 pair clusters.

Using the obtained CE effective interactions, we carried out Monte Carlo simulations using the program MultiComponent Easy Monte Carlo Code (Memc2) of ATAT.[64] Statistical samplings were performed in the canonical ensemble (*i.e.*, fixed composition) within a 40 × 40 × 1 supercell containing 3200 surface atoms. The Monte Carlo simulations were performed with target precision of 1 meV in the average energy. We started the simulation from high temperatures (5000 K) and gradually approached room temperature (300 K) with a temperature step of 200 K. These are used to study the distribution of adsorbants on the surface.

In order to evaluate the mixing and Gibbs free energies, work function, and lattice constants of the structures within different concentrations of functional groups, we generated representative supercell models and carried out separate DFT calculations for those. Following the same construction principles as in generating special quasi-random structures, but employing the correlations from the MC simulations instead of random correlations, we generated representative special quasi-ordered structures (SQoS) with 4 × 4 supercells.[65,66] These SQoS supercells are used to evaluate the final material properties.

ASSOCIATED CONTENT

Supporting Information

The Supporting Information is available free of charge on the ACS Publications website at DOI: 10.1021/acsnano.9b03511.

ATAT files (ZIP)

Additional details and all numerical values needed for the determination of chemical potentials of solutes; benchmarking of exchange-correlation functionals and the size of the cluster expansion; surface structures and energies for Ti_2C, similar to those for Ti_3C_2 presented in the main text (PDF)

AUTHOR INFORMATION

Corresponding Author

*E-mail: hannu-pekka.komsa@aalto.fi.

ORCID

Rina Ibragimova: 0000-0001-5773-3457

Martti J. Puska: 0000-0002-8419-3289

Hannu-Pekka Komsa: 0000-0002-0970-0957

Notes

The authors declare no competing financial interest.

Computational data generated in this study have been submitted to NOMAD repository and are available at http://dx.doi.org/10.17172/NOMAD/2019.07.02-1.

DOI: 10.1021/acsnano.9b03511
ACS Nano 2019, 13, 9171−9181

ACKNOWLEDGMENTS

We acknowledge funding from the Academy of Finland under Project No. 311058. We thank CSC Finland for generous grants of CPU time.

REFERENCES

(1) Manzeli, S.; Ovchinnikov, D.; Pasquier, D.; Yazyev, O. V.; Kis, A. 2D Transition Metal Dichalcogenides. *Nat. Rev. Mater.* **2017**, *2*, 17033.
(2) El-Kady, M. F.; Shao, Y.; Kaner, R. B. Graphene for Batteries, Supercapacitors and Beyond. *Nat. Rev. Mater.* **2016**, *1*, 16033.
(3) Chhowalla, M.; Shin, H. S.; Eda, G.; Li, L.-J.; Loh, K. P.; Zhang, H. The Chemistry of TwoDimensional Layered Transition Metal Dichalcogenide Nanosheets. *Nat. Chem.* **2013**, *5*, 263−275.
(4) Anasori, B.; Lukatskaya, M. R.; Gogotsi, Y. 2D Metal Carbides and Nitrides (MXenes) for Energy Storage. *Nat. Rev. Mater.* **2017**, *2*, 16098.
(5) Ghidiu, M.; Lukatskaya, M. R.; Zhao, M.-Q.; Gogotsi, Y.; Barsoum, M. W. Conductive TwoDimensional Titanium Carbide 'Clay' with High Volumetric Capacitance. *Nature* **2014**, *516*, 78−81.
(6) Zhang, C. J.; Anasori, B.; Seral-Ascaso, A.; Park, S.-H.; McEvoy, N.; Shmeliov, A.; Duesberg, G. S.; Coleman, J. N.; Gogotsi, Y.; Nicolosi, V. Transparent, Flexible, and Conductive 2D Titanium Carbide (MXene) Films with High Volumetric Capacitance. *Adv. Mater.* **2017**, *29*, 1702678.
(7) Cao, W.-T.; Chen, F.-F.; Zhu, Y.-J.; Zhang, Y.-G.; Jiang, Y.-Y.; Ma, M.-G.; Chen, F. Binary Strengthening and Toughening of MXene/Cellulose Nanofiber Composite Paper with NacreInspired Structure and Superior Electromagnetic Interference Shielding Properties. *ACS Nano* **2018**, *12*, 4583−4593.
(8) Hantanasirisakul, K.; Zhao, M.-Q.; Urbankowski, P.; Halim, J.; Anasori, B.; Kota, S.; Ren, C. E.; Barsoum, M. W.; Gogotsi, Y. Fabrication of $Ti_3C_2T_x$ MXene Transparent Thin Films with Tunable Optoelectronic Properties. *Adv. Electron. Mater.* **2016**, *2*, 1600050.
(9) Barsoum, M. W.; Radovic, M. Elastic and Mechanical Properties of the MAX Phases. *Annu. Rev. Mater. Res.* **2011**, *41*, 195−227.
(10) Xie, Y.; Naguib, M.; Mochalin, V. N.; Barsoum, M. W.; Gogotsi, Y.; Yu, X.; Nam, K.-W.; Yang, X.-Q.; Kolesnikov, A. I.; Kent, P. R. C. Role of Surface Structure on Li-Ion Energy Storage Capacity of Two-Dimensional Transition-Metal Carbides. *J. Am. Chem. Soc.* **2014**, *136*, 6385−6394.
(11) Naguib, M.; Kurtoglu, M.; Presser, V.; Lu, J.; Niu, J.; Heon, M.; Hultman, L.; Gogotsi, Y.; Barsoum, M. W. Two-Dimensional Nanocrystals Produced by Exfoliation of Ti_3AlC_2. *Adv. Mater.* **2011**, *23*, 4248−4253.
(12) Mashtalir, O.; Naguib, M.; Dyatkin, B.; Gogotsi, Y.; Barsoum, M. W. Kinetics of Aluminum Extraction from Ti_3AlC_2 in Hydrofluoric Acid. *Mater. Chem. Phys.* **2013**, *139*, 147−152.
(13) Shi, C.; Beidaghi, M.; Naguib, M.; Mashtalir, O.; Gogotsi, Y.; Billinge, S. J. L. Structure of Nanocrystalline Ti_3C_2 MXene Using Atomic Pair Distribution Function. *Phys. Rev. Lett.* **2014**, *112*, 125501.
(14) Persson, I.; Näslund, L.-Å.; Halim, J.; Barsoum, M. W.; Darakchieva, V.; Palisaitis, J.; Rosen, J.; Persson, P. O. Å. On the Organization and Thermal Behavior of Functional Groups on Ti_3C_2 MXene Surfaces in Vacuum. *2D Mater.* **2018**, *5*, No. 015002.
(15) Halim, J.; Cook, K. M.; Naguib, M.; Eklund, P.; Gogotsi, Y.; Rosen, J.; Barsoum, M. W. X-Ray Photoelectron Spectroscopy of Select Multi-Layered Transition Metal Carbides (MXenes). *Appl. Surf. Sci.* **2016**, *362*, 406−417.
(16) Mariano, M.; Mashtalir, O.; Antonio, F. Q.; Ryu, W.-H.; Deng, B.; Xia, F.; Gogotsi, Y.; Taylor, A. D. Solution-Processed Titanium Carbide MXene Films Examined as Highly Transparent Conductors. *Nanoscale* **2016**, *8*, 16371−16378.
(17) Wang, X.; Shen, X.; Gao, Y.; Wang, Z.; Yu, R.; Chen, L. Atomic-Scale Recognition of Surface Structure and Intercalation Mechanism of Ti_3C_2X. *J. Am. Chem. Soc.* **2015**, *137*, 2715−2721.
(18) Karlsson, L. H.; Birch, J.; Halim, J.; Barsoum, M. W.; Persson, P. O. Å. Atomically Resolved Structural and Chemical Investigation of Single MXene Sheets. *Nano Lett.* **2015**, *15*, 4955−4960.
(19) Wang, H.-W.; Naguib, M.; Page, K.; Wesolowski, D. J.; Gogotsi, Y. Resolving the Structure of $Ti_3C_2Ti_x$ MXenes through Multilevel Structural Modeling of the Atomic Pair Distribution Function. *Chem. Mater.* **2016**, *28*, 349−359.
(20) Hope, M. A.; Forse, A. C.; Griffith, K. J.; Lukatskaya, M. R.; Ghidiu, M.; Gogotsi, Y.; Grey, C. P. NMR Reveals the Surface Functionalisation of Ti_3C_2 MXene. *Phys. Chem. Chem. Phys.* **2016**, *18*, 5099−5102.
(21) Sang, X.; Xie, Y.; Lin, M.-W.; Alhabeb, M.; Van Aken, K. L.; Gogotsi, Y.; Kent, P. R. C.; Xiao, K.; Unocic, R. R. Atomic Defects in Monolayer Titanium Carbide ($Ti_3C_2T_x$) MXene. *ACS Nano* **2016**, *10*, 9193−9200.
(22) Xie, Y.; Kent, P. R. C. Hybrid Density Functional Study of Structural and Electronic Properties of Functionalized $Ti_{n+1}X_n$ (X = C, N) Monolayers. *Phys. Rev. B: Condens. Matter Mater. Phys.* **2013**, *87*, 235441.
(23) Khazaei, M.; Arai, M.; Sasaki, T.; Chung, C.-Y.; Venkataramanan, N. S.; Estili, M.; Sakka, Y.; Kawazoe, Y. Novel Electronic and Magnetic Properties of Two-Dimensional Transition Metal Carbides and Nitrides. *Adv. Funct. Mater.* **2013**, *23*, 2185−2192.
(24) Yu, Y.-X. Prediction of Mobility, Enhanced Storage Capacity, and Volume Change during Sodiation on Interlayer-Expanded Functionalized Ti_3C_2 MXene Anode Materials for SodiumIon Batteries. *J. Phys. Chem. C* **2016**, *120*, 5288−5296.
(25) Ashton, M.; Mathew, K.; Hennig, R. G.; Sinnott, S. B. Predicted Surface Composition and Thermodynamic Stability of MXenes in Solution. *J. Phys. Chem. C* **2016**, *120*, 3550−3556.
(26) Enyashin, A.; Ivanovskii, A. Atomic Structure, Comparative Stability and Electronic Properties of Hydroxylated Ti_2C and Ti_3C_2 Nanotubes. *Comput. Theor. Chem.* **2012**, *989*, 27−32.
(27) Hu, T.; Hu, M.; Gao, B.; Li, W.; Wang, X. Screening Surface Structure of MXenes by HighThroughput Computation and Vibrational Spectroscopic Confirmation. *J. Phys. Chem. C* **2018**, *122*, 18501−18509.
(28) Mishra, A.; Srivastava, P.; Carreras, A.; Tanaka, I.; Mizuseki, H.; Lee, K.-R.; Singh, A. K. Atomistic Origin of Phase Stability in Oxygen-Functionalized MXene: A Comparative Study. *J. Phys. Chem. C* **2017**, *121*, 18947−18953.
(29) Zhan, C.; Naguib, M.; Lukatskaya, M.; Kent, P. R. C.; Gogotsi, Y.; Jiang, D.-e. Understanding the MXene Pseudocapacitance. *J. Phys. Chem. Lett.* **2018**, *9*, 1223−1228.
(30) Cheng, Y.-W.; Dai, J.-H.; Zhang, Y.-M.; Song, Y. Two-Dimensional, Ordered, Double Transition Metal Carbides (MXenes): A New Family of Promising Catalysts for the Hydrogen Evolution Reaction. *J. Phys. Chem. C* **2018**, *122*, 28113−28122.
(31) Yoo, S.-H.; Todorova, M.; Neugebauer, J. Selective Solvent-Induced Stabilization of Polar Oxide Surfaces in an Electrochemical Environment. *Phys. Rev. Lett.* **2018**, *120*, No. 066101.
(32) Ashton, M.; Trometer, N.; Mathew, K.; Suntivich, J.; Freysoldt, C.; Sinnott, S. B.; Hennig, R. G. Predicting the Electrochemical Synthesis of 2D Materials from First Principles. *J. Phys. Chem. C* **2019**, *123*, 3180−3187.
(33) Yip, S. *Handbook of Materials Modeling*; Springer: Dordrecht, The Netherlands, 2007; pp 149−194.
(34) Todorova, M.; Neugebauer, J. Extending the Concept of Defect Chemistry from Semiconductor Physics to Electrochemistry. *Phys. Rev. Appl.* **2014**, *1*, No. 014001.
(35) Hu, T.; Li, Z.; Hu, M.; Wang, J.; Hu, Q.; Li, Q.; Wang, X. Chemical Origin of TerminationFunctionalized MXenes: $Ti_3C_2T_2$ as a Case Study. *J. Phys. Chem. C* **2017**, *121*, 19254−19261.
(36) Khazaei, M.; Arai, M.; Sasaki, T.; Ranjbar, A.; Liang, Y.; Yunoki, S. OH-Terminated TwoDimensional Transition Metal Carbides and Nitrides as Ultralow Work Function Materials. *Phys. Rev. B: Condens. Matter Mater. Phys.* **2015**, *92*, No. 075411.

DOI: 10.1021/acsnano.9b03511
ACS Nano 2019, 13, 9171−9181

(37) Xu, J.; Shim, J.; Park, J.-H.; Lee, S. MXene Electrode for the Integration of WSe2 and MoS2 Field Effect Transistors. *Adv. Funct. Mater.* **2016**, *26*, 5328−5334.
(38) Peng, C.; Wei, P.; Li, X.; Liu, Y.; Cao, Y.; Wang, H.; Yu, H.; Peng, F.; Zhang, L.; Zhang, B.; Lv, K. High Efficiency Photocatalytic Hydrogen Production over Ternary Cu/TiO2@$Ti_3C_2Ti_x$ Enabled by Low-Work-Function 2D Titanium Carbide. *Nano Energy* **2018**, *53*, 97−107.
(39) Kang, Z.; Ma, Y.; Tan, X.; Zhu, M.; Zheng, Z.; Liu, N.; Li, L.; Zou, Z.; Jiang, X.; Zhai, T.; Gao, Y. MXene-Silicon Van Der Waals Heterostructures for High-Speed Self-Driven Photodetectors. *Adv. Electron. Mater.* **2017**, *3*, 1700165.
(40) Wang, Z.; Kim, H.; Alshareef, H. N. Oxide Thin-Film Electronics using All-MXene Electrical Contacts. *Adv. Mater.* **2018**, *30*, 1706656.
(41) Ambrosio, F.; Guo, Z.; Pasquarello, A. Absolute Energy Levels of Liquid Water. *J. Phys. Chem. Lett.* **2018**, *9*, 3212−3216.
(42) Trasatti, S. The Absolute Electrode Potential: an Explanatory Note. *Pure Appl. Chem.* **1986**, *58*, 955−966.
(43) Zhang, C. J.; Pinilla, S.; McEvoy, N.; Cullen, C. P.; Anasori, B.; Long, E.; Park, S.-H.; SeralAscaso, A.; Shmeliov, A.; Krishnan, D.; Morant, C.; Liu, X.; Duesberg, G. S.; Gogotsi, Y.; Nicolosi, V. Oxidation Stability of Colloidal Two-Dimensional Titanium Carbides (MXenes). *Chem. Mater.* **2017**, *29*, 4848−4856.
(44) Chertopalov, S.; Mochalin, V. N. Environment-Sensitive Photoresponse of Spontaneously Partially Oxidized Ti_3C_2 MXene Thin Films. *ACS Nano* **2018**, *12*, 6109−6116.
(45) Hong Ng, V. M.; Huang, H.; Zhou, K.; Lee, P. S.; Que, W.; Xu, J. Z.; Kong, L. B. Recent Progress in Layered Transition Metal Carbides and/or Nitrides (MXenes) and Their Composites: Synthesis and Applications. *J. Mater. Chem. A* **2017**, *5*, 3039−3068.
(46) Hart, J. L.; Hantanasirisakul, K.; Lang, A. C.; Anasori, B.; Pinto, D.; Pivak, Y.; van Omme, J. T.; May, S. J.; Gogotsi, Y.; Taheri, M. L. Control of MXenes Electronic Properties Through Termination and Intercalation. *Nat. Commun.* **2019**, *10*, 522.
(47) Marcus, Y. The Thermodynamics of Solvation of Ions. Part 2.-The Enthalpy of Hydration at 298.15 K. *J. Chem. Soc., Faraday Trans. 1* **1987**, *83*, 339−349.
(48) Marcus, Y. Thermodynamics of Solvation of Ions. Part 5.-Gibbs Free Energy of Hydration at 298.15 K. *J. Chem. Soc., Faraday Trans.* **1991**, *87*, 2995−2999.
(49) Kresse, G.; Furthmüller, J. Efficient Iterative Schemes for *Ab Initio* Total-Energy Calculations Using a Plane-Wave Basis Set. *Phys. Rev. B: Condens. Matter Mater. Phys.* **1996**, *54*, 11169−11186.
(50) Perdew, J. P.; Burke, K.; Ernzerhof, M. Generalized Gradient Approximation Made Simple. *Phys. Rev. Lett.* **1996**, *77*, 3865−3868.
(51) Grimme, S.; Ehrlich, S.; Goerigk, L. Effect of the Damping Function in Dispersion Corrected Density Functional Theory. *J. Comput. Chem.* **2011**, *32*, 1456−1465.
(52) Perdew, J. P.; Ruzsinszky, A.; Csonka, G. I.; Vydrov, O. A.; Scuseria, G. E.; Constantin, L. A.; Zhou, X.; Burke, K. Restoring the Density-Gradient Expansion for Exchange in Solids and Surfaces. *Phys. Rev. Lett.* **2008**, *100*, 136406.
(53) Heyd, J.; Scuseria, G. E. Assessment and Validation of a Screened Coulomb Hybrid Density Functional. *J. Chem. Phys.* **2004**, *120*, 7274−7280.
(54) Sun, J.; Ruzsinszky, A.; Perdew, J. P. Strongly Constrained and Appropriately Normed Semilocal Density Functional. *Phys. Rev. Lett.* **2015**, *115*, No. 036402.
(55) Peng, H.; Yang, Z.-H.; Perdew, J. P.; Sun, J. Versatile van der Waals Density Functional Based on a Meta-Generalized Gradient Approximation. *Phys. Rev. X* **2016**, *6*, No. 041005.
(56) Zha, X.-H.; Luo, K.; Li, Q.; Huang, Q.; He, J.; Wen, X.; Du, S. Role of the Surface Effect on the Structural, Electronic and Mechanical Properties of the Carbide MXenes. *EPL (Europhysics Letters)* **2015**, *111*, 26007.
(57) Wang, S.; Li, J.-X.; Du, Y.-L.; Cui, C. First-Principles Study on Structural, Electronic and Elastic Properties of Graphene-like Hexagonal Ti_2C Monolayer. *Comput. Mater. Sci.* **2014**, *83*, 290−293.
(58) Er, D.; Li, J.; Naguib, M.; Gogotsi, Y.; Shenoy, V. B. Ti3C2MXene as a High Capacity Electrode Material for Metal (Li, Na, K, Ca) Ion Batteries. *ACS Appl. Mater. Interfaces* **2014**, *6*, 11173−11179.
(59) Togo, A.; Tanaka, I. First Principles Phonon Calculations in Materials Science. *Scr. Mater.* **2015**, *108*, 1−5.
(60) Mathew, K.; Kolluru, V. S. C.; Hennig, R. G. VASPsol: Implicit Solvation and Electrolyte Model for Density-Functional Theory; https://github.com/henniggroup/VASPsol (accessed March 23, 2019).
(61) Mathew, K.; Sundararaman, R.; Letchworth-Weaver, K.; Arias, T. A.; Hennig, R. G. Implicit Solvation Model for Density-Functional Study of Nanocrystal Surfaces and Reaction Pathways. *J. Chem. Phys.* **2014**, *140*, No. 084106.
(62) van de Walle, A.; Ceder, G. Automating First-Principles Phase Diagram Calculations. *J. Phase Equilib.* **2002**, *23*, 348−359.
(63) van de Walle, A. Multicomponent Multisublattice Alloys, Nonconfigurational Entropy and Other Additions to the Alloy Theoretic Automated Toolkit. *CALPHAD: Comput. Coupling Phase Diagrams Thermochem.* **2009**, *33*, 266−278.
(64) van de Walle, A.; Asta, M. Self-Driven Lattice-Model Monte Carlo Simulations of Alloy Thermodynamic Properties and Phase Diagrams. *Modell. Simul. Mater. Sci. Eng.* **2002**, *10*, 521−538.
(65) Zunger, A.; Wei, S.-H.; Ferreira, L. G.; Bernard, J. E. Special Quasirandom Structures. *Phys. Rev. Lett.* **1990**, *65*, 353−356.
(66) Liu, J.; Fernández-Serra, M. V.; Allen, P. B. Special Quasiordered Structures: Role of ShortRange Order in the Semiconductor Alloy $(GaN)_{1-x}$ $(ZnO)_x$. *Phys. Rev. B: Condens. Matter Mater. Phys.* **2016**, *93*, No. 054207.

DOI: 10.1021/acsnano.9b03511
ACS Nano 2019, 13, 9171−9181